ARTICLE OPEN

Check for updates

# Flexible magnetoelectric complex oxide heterostructures on muscovite for proximity sensor

Yong-Jyun Wang[1], Jia-Wei Chen[2], Yu-Hong Lai[2], Pao-Wen Shao[2], Yugandhar Bitla[3], Yi-Chun Chen[4] and Ying-Hao Chu[1,2]✉

In modern technology, recent advances in multi-functional devices are rapidly developed for the diverse demands of human beings. Meanwhile, durability and adaptability to extreme environmental conditions are also required. In this study, a flexible magnetoelectric (ME) heterostructure based on $CoFe_2O_4$/$Pb(Zr,Ti)O_3$ composite thin film on muscovite is presented, with two geometries of the constituents, namely laminar heterostructure, and vertical nanostructure, adopted for the comparison. On the other hand, credited to the mechanical flexibility of muscovite, the impact of flexibility on ME properties is also discussed with a series of bending tests. Moreover, the ME response sustains for 10,000 times bending without significant decrease, validating the mechanical durability of this heterostructure on muscovite. With these advantages, a flexible proximity sensor based on this heterostructure is demonstrated for motion detection. It is expected to offer a pathway for creating the next-generational flexible devices, showing potential for future practical application.

*npj Flexible Electronics* (2023)7:10; https://doi.org/10.1038/s41528-023-00241-8

## INTRODUCTION

In the mighty torrent of history, the development of material technology usually determines the era's trend. With the evolution of time, the demand for contemporary technology is getting more and more diverse. Thus, exploring material systems is crucial to open ages for creating next-generational electronics. Recently, the exploration and discovery of ME systems have triggered intensive research due to their intriguing features and potential for practical applications. With rapid development, the manipulation of magnetic and electric orders is getting faster and more precise, which can also be applied to the Internet-of-things (IoT) field. This program delivers an idea for the revolution of rapid computation, offering a practical breakthrough for intelligent devices. Recent advances in the technologies involved with soft materials and system integration have paved the way for designing various types of flexible devices for practical applications, such as wearable electronics or flexible displays. With a combination of material systems and soft technology[1–3], many technical difficulties will be circumvented, and more potential applications can be delivered.

The magnetoelectric (ME) effect[4–6], defined as the coupling of electric and magnetic orders, allows the alternation of electrical polarization (magnetization) by an applied magnetic (electric) field. The multi-phase ME materials composed of magnetostrictive and piezoelectric components have triggered intensive attention due to their large strain-mediated magnetoelectric coupling over single-phase ones delivering a feasible way for practical applications in broadband sensors[7], actuators[8], memories[9] and energy storage devices[10]. The ME property can further be tuned by the choice and volume fractions of the constituents and the composite architecture. In many ME-related studies, ceramic materials are best known for their intriguing properties[11,12]. However, the fatal flaws of ceramic materials are their fragility and undesirable interface, hindering device performance[13]. Thus, there are two critical factors: mechanical flexibility and interfacial quality. Recent advance in the flexible ME system has demonstrated the tremendous response with the combination of alloy[14], polymers[15], and some composite[16] materials. Nonetheless, this work aims to build a flexible ceramic ME system using the two-dimensional (2D) layered muscovite as the substrate due to its superior mechanical flexibility and high thermal and chemical stability. These advantages enable muscovite to be a platform for studying the impact of flexibility on ME coupling. Moreover, the epitaxial growth of numerous materials on muscovite *via* quasi-van der Waals epitaxy has been demonstrated[17–19]. This fact assures the interfacial quality for 3D/2D heterostructures[20]. On the other hand, highly flexible functional materials are needed to acquire material properties. Among them, spinel cobalt ferrite ($CoFe_2O_4$, CFO) and perovskite lead zirconate titanate ($PbZr_{0.52}Ti_{0.48}O_3$, PZT) are selected due to their high lattice compatibility[21,22]. First, to increase the sensitivity to an external magnetic field, CFO with a strong magnetostriction effect is a suitable material as the magnetic component. Besides, CFO has more considerable electrical resistance than other alloy systems, reducing the negative impact on output voltage caused by leakage current; Piezoelectricity in PZT has been studied for decades and demonstrated to be solid and stable[23,24]. In addition, PZT with a high Curie temperature (~390 °C) enables itself to sustain external thermal disturbance[25]. The combination of PZT and CFO is chosen as a model system to exhibit magnetoelectric coupling on the muscovite substrate.

The inherent qualitative coupling between CFO and PZT phases induces an output voltage by an external magnetic field. The schematic diagram of the proximity sensor based on this ME system is illustrated in Fig. 1a. The architecture covers the magnetic and electric orders and $SrRuO_3$ (SRO) bottom electrodes for signal detection. However, a wide variety of oxide architectures can be obtained by process tuning[26], providing a pathway to explore the impact of different microstructures. The ME coupling effect happens at the interfaces between CFO and PZT, which

[1]Department of Materials Science and Engineering, National Tsing Hua University, Hsinchu 30013, Taiwan. [2]Department of Materials Science and Engineering, National Yang Ming Chiao Tung University, Hsinchu 30010, Taiwan. [3]Department of Physics, School of Physical Sciences, Central University of Rajasthan, Ajmer 305817, India. [4]Department of Physics, National Cheng Kung University, Tainan, Taiwan. ✉email: yhchu@mx.nthu.edu.tw

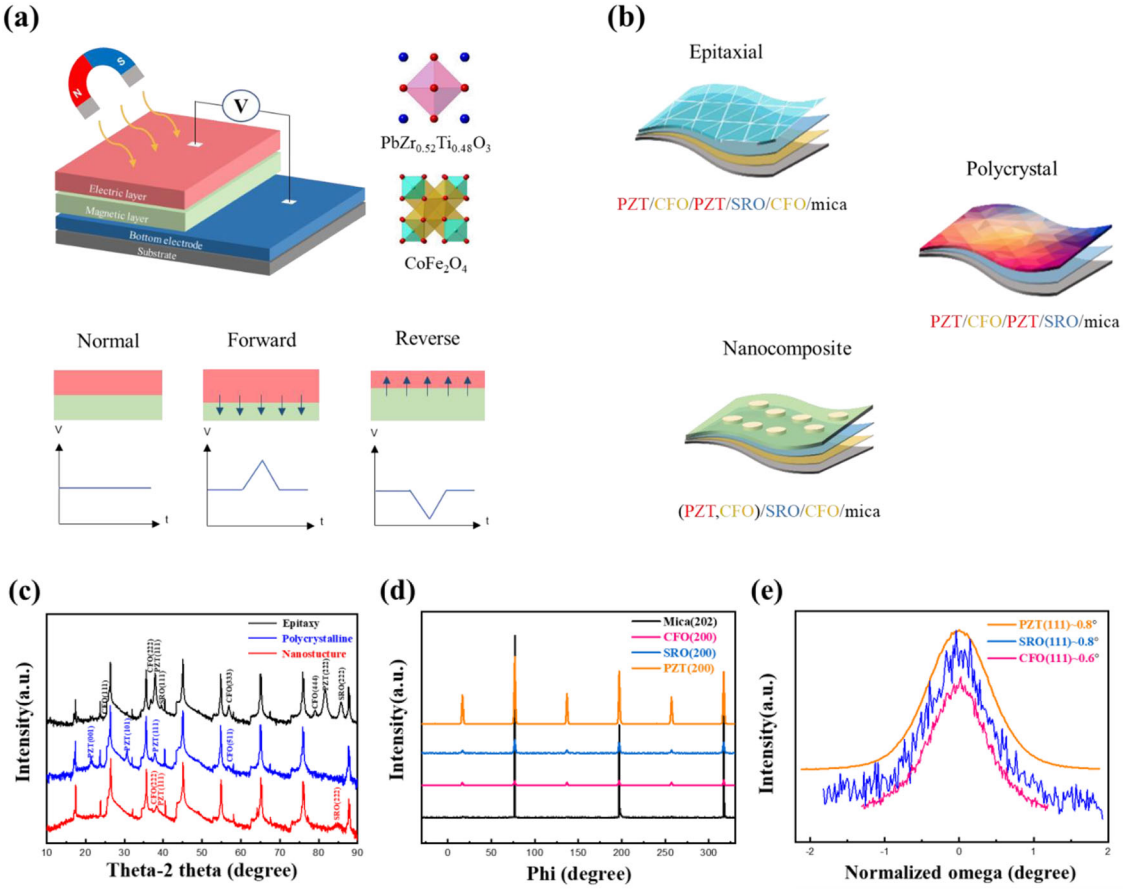


**Fig. 1 Structure and device design. a** Schematic interaction between magnetostriction and piezoelectric parts and the design of proximity sensing device. **b** Crystal structure of 2-2 (layer-by-layer PZT/CFO/PZT) and 1-3 (PZT, CFO) nanostructure with two different growth mechanisms. **c** Out-of-plane XRD 2θ-θ scan of the heterostructures. **d** Phi scans of muscovite {202}, CFO {200}, SRO {200} and PZT {200}. **e** Rocking curves of PZT (222), SRO (111), and CFO (111).

means that the performance is strongly affected by different geometries and material arrangements. The different design of the ME composite architecture depends on the connectivity of materials, such as 0-0, 0–3, 1–3, 3-1and 2-2, where the number indicates the dimension of the ferroelectric and magnetic components. The most commonly used ME architecture with successfully proven enhanced ME properties is 0–3 particle composite (the magnetic nanoparticles dispersed in the ferro-magnetic matrices), 1-3 vertical composite (the nanopillars embedded in the matrices), and 2-2 layered composite (the composite with alternate stacking of ferroelectric and magnetic layers). Thus, three architectures are designed, as shown in Fig. 1b, including 2-2 epitaxial, polycrystalline, and 1–3 nanostructure heterostructures. X-ray diffraction (XRD) and transmission electron microscopy (TEM) were used for structural characterization in this work. Electrical polarization and magnetization were studied on three ME heterostructures through the polarization-electric field (P-E) and magnetic-hysteresis (M-H) measurements. For the measurement of ME response, the magnetoelectric coefficient can be achieved by the electrical measurement system with an external DC magnetic field. Moreover, the influence of flexibility on ME response is also discussed in this work, which was implemented using the static and dynamic bending stages. In addition to the fundamental multiferroic study of CFO and PZT, a focus on the application of ME coupling was also carried out. A flexible ME-type proximity sensor is presented for motion detection application, suggesting potential for practical use. In conclusion, this work successfully uses the 2D muscovite to investigate the ME response of three different heterostructures along with the influence of flexibility, offering an opportunity to explore the intriguing mechanism inside.

## RESULTS AND DISCUSSION

### Structural analyses

In the first part, structure characteristics were examined to prove the correctness of phases. The XRD θ-2θ scan of the black line in Fig. 1c results from PZT/CFO/PZT/SRO/CFO/muscovite along the out-of-plane (OOP) direction. The observation of a series of diffraction peaks, including muscovite{001}, SRO{111}, CFO{111}, and PZT{111}, indicates the possible epitaxial feature of the heterostructure. The CFO buffered layer was removed from the mezzanine of SRO and muscovite substrate to obtain the polycrystalline growth. The OOP XRD pattern of PZT/CFO/PZT/SRO/muscovite (the blue line in Fig. 1c) shows PZT (001), (101), (111), and CFO (511) diffraction peaks, revealing the polycrystalline nature of the constituents with multi-orientations. A dual-target deposition of PZT and CFO was adopted to grow the nanostructure. The red line in Fig. 1c shows the XRD pattern of (PZT, CFO)/SRO/CFO/muscovite. There exist only SRO (222), CFO (222), and PZT (111) diffraction peaks without a secondary phase. In-plane (IP) Φ-scan measurement of the epitaxial system was conducted to confirm the epitaxial relationship further. The Φ-scans of muscovite{001}, SRO{111}, CFO{111}, and PZT{111} were used to determine the IP orientation, as shown in Fig. 1d. The three-fold symmetry along (111) orientation is observed, and three sets of peaks at 120° intervals are displayed. The feature of

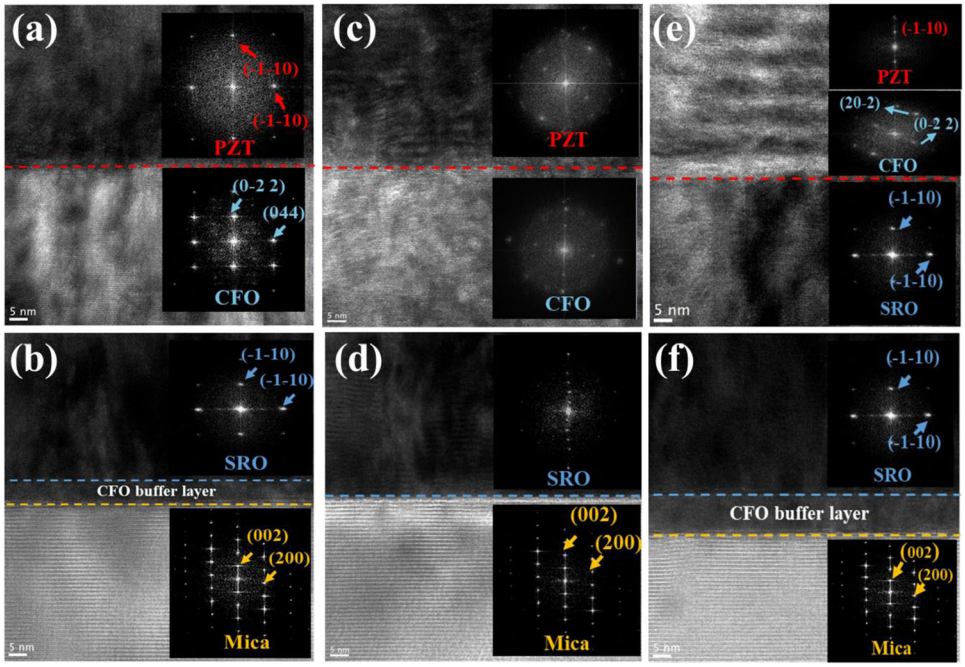


**Fig. 2 The cross-sectional TEM images with the FFT diffraction patterns and the EDS mapping of three structures.** The TEM images with the FFT diffraction patterns of **a**, **b** epitaxial, **c**, **d** polycrystalline, and **e, f** nanostructure heterostructures.

aligned peaks leads to the epitaxial relationship of the heterostructure as (111) PZT//(111) CFO// (111) PZT //(111) SRO//(111) CFO//(001) muscovite. Moreover, the performance of thin film dramatically depends on the crystal quality. Thus, the rocking curve measurements were conducted, and the full width at half maximum (FWHM) of PZT (111), SRO (111), and CFO (111) peaks are ~0.8°, ~0.8°, and ~0.6°, respectively, as shown in Fig. 1e, proving the crystal quality of the thin film.

Further, the microstructure of all the heterostructures was examined by transmission electron microscopy (TEM), as shown in Fig. 2. Meanwhile, the observation of the overall multilayer stack and the vertical structure can be seen in the low mag images in Supplementary Fig. 1, offering an opportunity to compare the interface quality. The cross-sectional TEM images of the epitaxial sample are shown in Fig. 2a, b, revealing the clear interfaces. The reciprocal lattices in the fast Fourier transform (FFT) patterns of PZT, CFO, SRO, and muscovite in the insets are indexed, delivering epitaxial features. The polymorphism of another sample was identified next. The corresponding FFT pattern in Fig. 2c, d presents the diffraction rings related to PZT, CFO, and SRO, indicating the polycrystalline feature of the heterostructure. Finally, the phases of CFO and PZT in the nanostructure were observed. From Fig. 2e, f, the FFT patterns of SRO, CFO (buffered layer), and muscovite are identical to the epitaxial one. As for the nanostructure sample, the EDS mapping of the whole structure in Supplementary Fig. 2 indicates no clear phase separation in the cross-sectional TEM images. However, the FFT pattern for PZT and CFO can still be captured. Such observation is constructive for the comparison and discussion in the later parts.

## Electrical and magnetic properties

Since the feature of crystal structure has been confirmed after a series of structural analyses, attention is now paid to the physical properties of the heterostructures. First, the ferroelectricity of the PZT phase should be examined to characterize the existence of electric polarization. According to the linear relation between electric polarization and piezoelectricity[27,28], the polarization's magnitude suggests the electrical contribution to magnetoelectric coupling. Therefore, P-E loops were measured in the unbent and bent conditions[29]. The maximum magnitude of the applied electric field was ~ ±560 kV cm$^{-1}$. The typical P-E hysteresis loops in Fig. 3a with a sharp change in polarization show a practical switching of dipoles. The epitaxial (red line) and polycrystalline (yellow line) heterostructures exhibit maximum polarization ($P_{max}$) of 61 μC cm$^{-2}$ and 61.2 μC cm$^{-2}$, respectively, while the nanostructure (blue line) has a lower $P_{max}$ of 28.1 μC cm$^{-2}$. Different performance among these three samples is attributed to structural order differences. There is no noticeable difference in the saturation polarization between the epitaxial and polycrystalline PZT layers. However, the coercive field of the epitaxial sample (102.5 kV cm$^{-1}$) is smaller than the polycrystalline form (145.5 kV cm$^{-1}$), indicating that the ability of dipole-switching depends on the uniformity of dipoles. As for the $P_{max}$ of the nanostructure, there is a 54% reduction compared to the epitaxial and polycrystalline samples. This decline originates from the chaotic arrangement of internal dipoles that hinders the net polarization. Furthermore, the switching behavior of ferroelectric domains in three architectures was investigated *via* piezoresponse force microscopy (PFM), as shown in Supplementary Fig. 3. The butterfly-shaped curves are indicative of domain switching. Furthermore, the information of positive $d_{33}$ can be obtained through PFM loops, providing strong evidence of piezoelectricity. After realizing the basic ferroelectricity, the stability of a flexible device to withstand mechanical bending is essential. Figure 3b shows the P-E hysteresis loops of PZT layers on muscovite under compression and tension. The stable remnant and maximum polarization ($P_r$ and $P_{max}$) values were observed under a bending radius of 5 mm. This result indicates that the flexible heterostructures could retain their original ferroelectricity even under mechanical constraints.

Having demonstrated the electrical properties, the magnetism in the designed systems was further investigated. The room temperature magnetic hysteresis loops were measured by vibrating sample magnetometer (VSM) by applying the magnetic field parallel (IP) and perpendicular (OOP) to the plane of the heterostructures. The typical magnetic hysteresis loops are shown in Fig. 3c and exhibit isotropic magnetic properties.

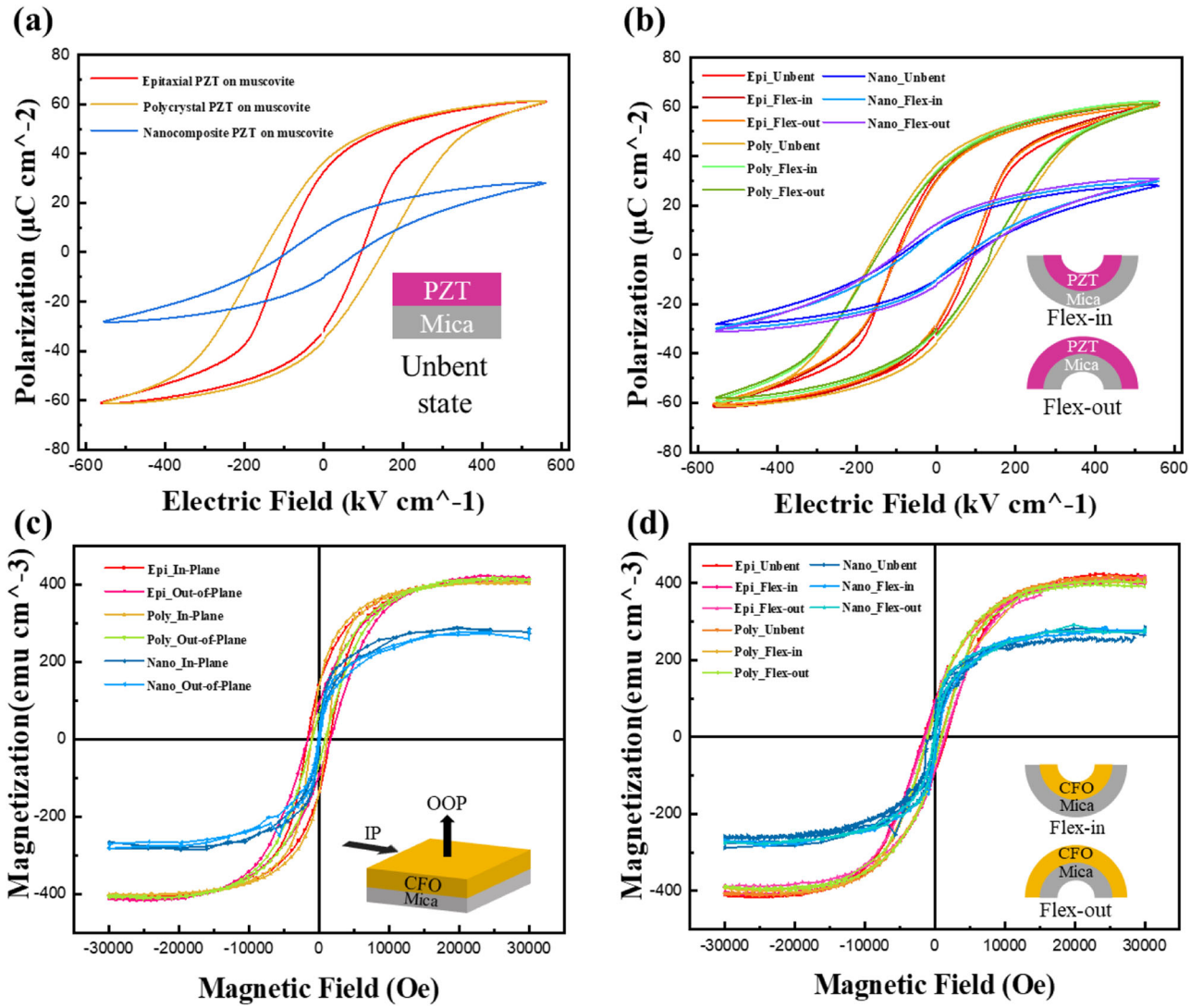


**Fig. 3 The PE loop and MH loop measurements for three samples on the muscovite substrate. a**, **b** PE loop measurement for PZT in unbent conditions and under compressive and tensile constraints. **c** MH loop for CFO along OOP and IP directions without bending. **d** MH loop for CFO under bending condition along OOP direction.

This is attributed to the growth direction of the CFO as it needs to be fully aligned to the magnetic easy axis along [001][30]. The saturation magnetization for the epitaxial and polycrystalline samples is around ~400 emu $cm^{-3}$, close to bulk value, while the nanostructure displays ~280 emu $cm^{-3}$. This result is consistent with the observation of distributed magnetic domains in the magnetic force microscopic (MFM) images, as shown in Supplementary Fig. 4. Furthermore, the effect of mechanical strain (compressive and tensile) on the magnetic properties of these heterostructures is depicted in Fig. 3d. It can be noticed that there is no significant change in the magnetic behavior of heterostructure no matter how it bends due to the mechanical flexibility and extraordinary extensibility supplied by the muscovite substrate. In addition, the high-temperature resilience and chemical stability of underlying muscovite substrates allow the heterostructure operation in such constraints not possible with the heterostructures realized on conventional polymer-based flexible substrates. From device programming, the isotropic electric and magnetic properties would make the device more comprehensive without considering the orientation issue.

## Magnetoelectric properties

After validating the electric and magnetic properties, the ME coupling of these heterostructures was investigated. The ME effect usually emerges due to intimate elastic coupling across the interfaces between the magnetostriction effect of CFO and the piezoelectric effect of PZT[31]. In general, the magnetoelectric coefficient $\alpha_E$ is given by[32],

$$\alpha_E = \Delta E\, \Delta H^{-1} = \Delta V\, \Delta H^{-1}\, t^{-1}$$

Where V is the output voltage, H is the applied magnetic field, and t is the total thickness of the thin film. This equation provides a macroscopic view of the ME coupling effect. The performance on the $\alpha_E$ of three heterostructures and their corresponding output voltage in the unbent state, along with the increasing DC magnetic field, is shown in Fig. 4a–c. The maximum values of $\alpha_E$ in the epitaxial, polycrystalline, and nanostructure systems are 84.3, 74.4, and 34.5 mV $Oe^{-1}$ $cm^{-1}$. Among these, the epitaxial one exhibits the most significant macroscopic ME coupling coefficient, which can be attributed to the uniformity of its crystal structure. Furthermore, the stacking feature of a 2-2 layered structure is more beneficial for longitudinal ME coupling than other

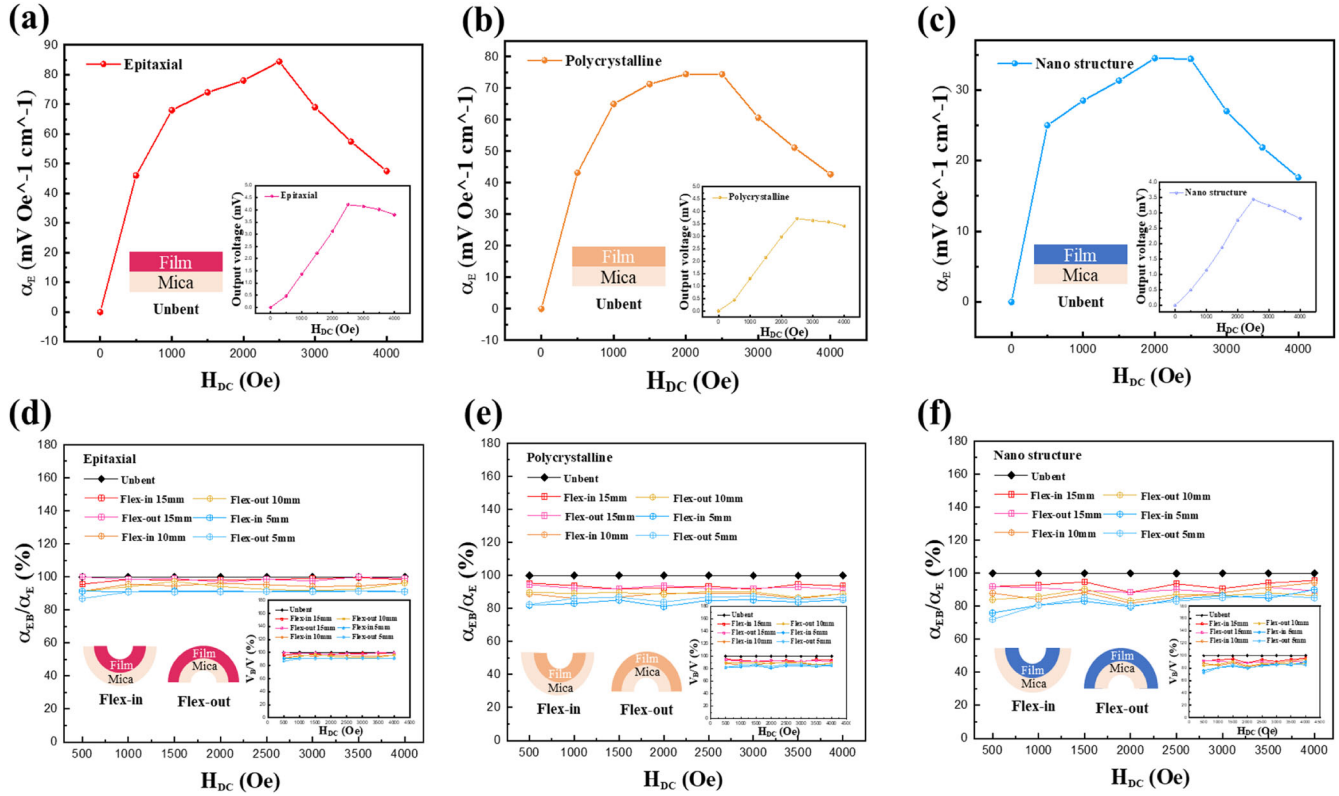


**Fig. 4 ME coupling effect measurement with reliable and bending tests. a–c** $\alpha_E$, the corresponding output voltage in three heterostructures, and the increasing DC magnetic field. **d–f** Deviation for epitaxial, polycrystalline, and nanostructure samples under compressive and tensile strains from the bending radius of 15 mm to 5 mm.

architectures due to the interfacial anisotropy. Besides, both $\alpha_E$ and output voltage first increase and then decrease along with the increasing DC-triggered magnetic field. This phenomenon is due to the saturating magnetostriction, which can be observed in the MH loops in Fig. 3c. On the other hand, the influence of flexibility on $\alpha_E$ is also investigated in this study. The result of bending tests shown in Fig. 4d–f provides information on how these three heterostructures work against mechanical constraints. The samples were placed on a series of solid bending stages with curvature from 15 mm to 5 mm (Supplementary Fig. 5). According to the result, a progressive decay of $\alpha_E$ along with the decrease of bending radius can be observed in each architecture. Although there is no remarkable difference in the P-E and M-H loop measurements, the maximum deviation of $\alpha_E$ is 16, 19, and 28% in epitaxial, polycrystalline, and nanostructure, which can be attributed to the different pathways for sustaining the mechanical strain. The various interface designs between 2-2 and 1-3 heterostructures significantly impact the sensitivity of $\alpha_E$ to bending radius, reflecting the different performance in the ME coupling. For the ME coupling, it happens at the interfaces between the magnetic (CFO) and electrical (PZT) phases. The strain induced by the bent state strongly influences the ME coupling, which may hinder the interaction between PZT and CFO. As a result, the increasing mechanical strain along with the bending curvature corresponds to the progressive decay of $\alpha_E$ under the bent state in the results. This can be used as an indication of how the mechanical strain influences the $\alpha_E$ for different heterostructures. Moreover, the result of the cycling test is also provided in Supplementary Fig. 6 to examine the stability of properties. The decay of $\alpha_E$ is no more than 8% after 10000 cycles of bending in three heterostructures, implying that the $\alpha_E$ is robust against the mechanical constraint due to the epitaxy nature of muscovite.

## Demo of motion detection

After analyzing magnetoelectric properties, it is critical to explore the potential application of this flexible magnetoelectric heterostructure on muscovite for further commercialization or practical use. Thus, a flexible proximity sensor demo is presented, with the schematic diagram shown in Fig. 5a. The proximity sensor can be further applied in motion detection with mechanical flexibility. Figure 5b depicts the result of the demonstration corresponding to the pictures in Fig. 5c. The film was mounted on one side of the finger, while the external magnet was installed on the opposite side. Once the two fingers are approaching and removing, the signal can help to distinguish the motion. The opposite tips of the signal represent the swing of two fingers back and forth for about 30 s. This implies that the directional interpretation of our proximity sensor is precise and instant, increasing the accuracy of gesture detection and invoking more potential applications in motion detection. Such performance can be attributed to the mechanical strength and extensibility of the muscovite substrate, decreasing the damage to the structure and retaining its optimal behaviors.

In summary, we have demonstrated a flexible ME system in three distinct architectures, including epitaxial, polycrystalline, and nanostructure, on muscovite consisting entirely of ceramic materials (CFO and PZT) and its potential application as a proximity sensor. The crystal structure, crystalline quality, and microstructure of these ME heterostructures were characterized and compared through the analysis of XRD and TEM. In this part, the three different peak sets in XRD help to initially distinguish the crystal planes with their symmetry and prove the correctness of phases. The 2-2 layered architecture of epitaxial and polycrystalline heterostructures and the 1-3 nanostructure with intertwined PZT and CFO can be observed from the cross-sectional TEM images. Moreover, with the help of FFT diffraction patterns, the

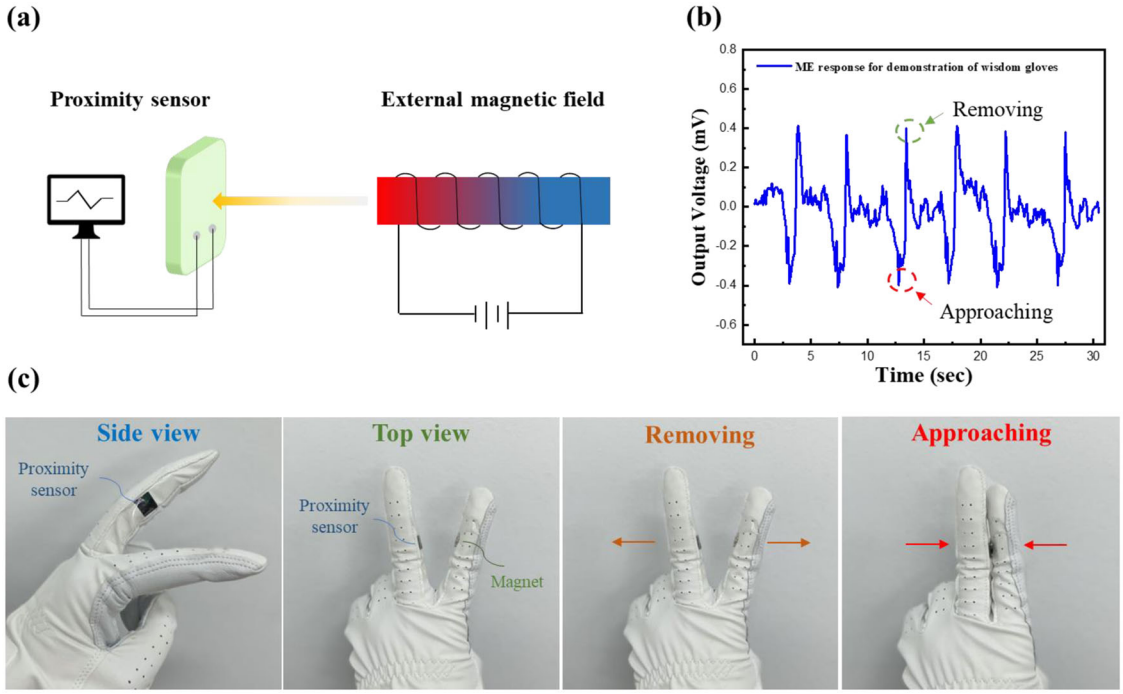


**Fig. 5 Demonstration for remote motion detection via intelligent gloves. a** The schematic diagram of the layout. **b**, **c** The result and corresponding figures for motion detection show that two fingers swing back and forth for about 30s.

microstructural properties of three heterostructures were also well characterized. The P-E and M-H loop measurements reveal the three heterostructures' electrical and magnetic properties to identify the polarization of PZT and the magnetization of CFO, respectively. Based on the results, the maximum polarization and magnetization of epitaxial and polycrystalline heterostructures are about the same, and the difference between them is at the coercive fields; At the same time, the nanostructure sample presents the smaller values in the maximum polarization and magnetization. We conclude that the reason can be attributed to the arrangement of crystals, which strongly influences the flip of domains. Meanwhile, the results of P-E and M-H loop measurements under bent conditions suggest robust properties even under mechanical constraints. The performance of strain-mediated ME coupling in three architectures is compared after a series of measurements. Among them, the $\alpha_E$ in the epitaxial one is the highest and lowest in the nanostructure. Due to the interfacial anisotropy, we believe that the respectively continuous interfaces in the 2-2 architecture are more beneficial for the ME coupling. On the other hand, the interfaces in the 1-3 nanostructure are much vaguer than the 2-2 one, hindering the interaction of magnetic and electrical orders. For the discussion of $\alpha_E$ against mechanical constraint, the bending and cycling tests on ME properties were implemented. From the result, a systematic bending test can analyze the impact of mechanical strain on $\alpha_E$. The progressive decay and increasing bending curvatures can be observed, though this phenomenon was not presented in the P-E and M-H, respectively. Such a phenomenon results from the compressive and tensile strain induced by the bending condition. The applied strain will significantly hinder the coupling between the PZT and CFO, contributing to the decrease of the $\alpha_E$ value in the three architectures. The durability of this heterostructure on muscovite is relatively high due to the stability after 10000 times of cycling bending. In a nutshell, this work delivers an idea to explore the ME properties based on the heterostructures of flexible muscovite. Furthermore, the demonstration of flexible proximity sensors applied in motion detection shows potential in practical use, which is compatible with intelligent wearable systems in magnetoception, healthcare, security, internet-of-things, and energy harvesting.

## METHODS

### Sample preparation

Three different heterostructures were all fabricated on (001) muscovite substrate using pulsed laser deposition[33,34]. The polycrystalline PZT, CFO, and SRO targets were prepared by the solid-state reaction method. Mica substrates cut into 1 cm × 1 cm with 30 μm thickness were purchased from Taiwan Epitaxial Thin Film Corporation Limited. A CFO interfacial buffer layer was deposited initially, followed by the SRO bottom electrode and the PZT-CFO layers to fabricate the epitaxial sample. As for the polycrystalline sample, the same approach without a CFO buffer layer was followed. The nanocomposite structure was obtained by the sequential dual-target deposition method. Using a KrF excimer laser (λ = 248 nm, Lambda Physic) operated at a 20 Hz repetition rate. The energy density of 2.5 J cm−2, the deposition process of 2-2 structure was carried out in 100 mtorr and 630 °C for SRO, 120 mtorr and 570 °C for PZT, 20 mtorr and 650 °C for CFO. The oxygen atmosphere and substrate temperature during the dual-target deposition method were 100 mtorr and 590 °C. PZT and CFO targets were allowed to be hit by desired laser pulses, alternatively using a computer-controlled rotation stage. At last, the Pt top circular electrode with a diameter of 200 μm was deposited at room temperature by the radio frequency sputter method.

### Structural analysis

The room temperature θ−2θ normal direction scan, phi scan, and rocking curve measurements were conducted by the Bruker D8 Discover XRD System, which uses Cu Kα radiation to obtain structural information. The cross-sectional TEM images were captured on specimens fabricated using the focused ion beam technique in the FEI Helios G4 system, including a low-pressure polishing process at 5 and 2 keV.

### Electrical properties

The P-E loop measurements were performed under 100 mV alternating voltage, 5 kHz AC frequency, and the electric field was applied from $-560\ kV\ cm^{-1}$ to $560\ kV\ cm^{-1}$.

### Magnetic properties

The room temperature M-H loop measurements were performed by Quantum design VSM in magnetic fields.

### Magnetoelectric measurements

Two enameled wires were connected to samples by Ag paste, with one side connecting to the bottom electrode part and the other relating to the functional element. ME coupling measurements were then performed by Laboratory Virtual Instrumentation Engineering Workbench (LabVIEW) along with the applied DC magnetic field.

## DATA AVAILABILITY

The corresponding author's data supporting this study's findings are available upon reasonable request.

Received: 23 September 2022; Accepted: 25 January 2023;
Published online: 18 February 2023

## REFERENCES

1. Bitla, Y. & Chu, Y. H. MICAtronics: A new platform for flexible X-tronics. *FlatChem* **3**, 26–42 (2017).
2. Yang, N. et al. Ultrasensitive flexible magnetoelectric sensor. *APL Mater.* **9**, 021123 (2021).
3. Zhang, X., Ai, J., Zou, R. & Su, B. Compressible and stretchable magnetoelectric sensors based on liquid metals for highly sensitive, self-powered respiratory monitoring. *ACS Appl. Mater. Interfaces* **13**, 15727–15737 (2021).
4. Spaldin, N. A. & Ramesh, R. Advances in magnetoelectric multiferroics. *Nat. Mater.* **18**, 203–212 (2019).
5. Eerenstein, W., Mathur, N. D. & Scott, J. F. Multiferroic and magnetoelectric materials. *Nature* **442**, 759–765 (2006).
6. Fiebig, M. Revival of the magnetoelectric effect. *J. Phys. D.* **38**, R123 (2005).
7. Kumar, A. & Kaur, D. Magnetoelectric heterostructures for next-generation MEMS magnetic field sensing applications. *J. Alloy. Compd.* **897**, 163091 (2022).
8. Yang, Y., Wu, H. & Yang, B. Self-sensing nanometric magnetoelectric actuator based on Metglas/PZT composites. *ACTUATOR*. **2021**, 1–4 (2021).
9. Kosub, T. et al. Purely antiferromagnetic magnetoelectric random access memory. *Nat. Commun.* **8**, 13985 (2017).
10. Srinivasan, G. Magnetoelectric composites. *Annu. Rev. Mater. Res.* **40**, 153–178 (2010).
11. Liang, K. C. et al. Giant magnetoelectric effect in $HoAl_3(BO_3)_4$. *Phys. Rev. B.* **83**, 180417 (2011).
12. Lin, Y., Cai, N., Zhai, J., Liu, G. & Nan, C. W. Giant magnetoelectric effect in multiferroic laminated composites. *Phys. Rev. B.* **72**, 012405 (2005).
13. Martins, P. & Lanceros-Méndez, S. Polymer-based magnetoelectric materials. *Adv. Funct. Mater.* **23**, 3371–3385 (2013).
14. Staaf, H. et al. High magnetoelectric coupling of Metglas and P (VDF-TrFE) laminates. *Sci. Rep.* **12**, 1–7 (2022).
15. Long, Y. et al Giant zero-biased magnetoelectric coupling characteristics in flexible Metglas/poly (vinylidene fluoride) heterostructures. *IEEE.* **2018**, 1–1 (2018).
16. Pereira, N., Lima, A. C., Lanceros-Mendez, S. & Martins, P. Magnetoelectrics: Three centuries of research heading towards the 4.0 industrial revolution. *Mater* **13**, 4033 (2020).
17. Bitla, Y. et al. Oxide heteroepitaxy for flexible optoelectronics. *ACS Appl. Mater. Interfaces* **8**, 32401–32407 (2016).
18. Ma, C. H. et al. Transparent antiradiative ferroelectric heterostructure based on flexible oxide heteroepitaxy. *ACS Appl. Mater. Interfaces* **10**, 30574–30580 (2018).
19. Wu, P. C. et al. Heteroepitaxy of $Fe_3O_4$/muscovite: A new perspective for flexible spintronics. *ACS Appl. Mater. Interfaces* **8**, 33794–33801 (2016).
20. Yen, M., Bitla, Y. & Chu, Y. H. Heteroepitaxy of $Fe_3O_4$/Muscovite: A New Perspective for Flexible Spintronics. *Mater. Chem. Phys.* **234**, 185–195 (2019).
21. Zheng, H. et al. Giant room temperature magnetoelectric response in strain-controlled nanocomposites. *Nano Lett.* **6**, 1401–1407 (2016).
22. Yan, L. et al. Review of magnetoelectric perovskite–spinel self-assembled nanocomposite thin films. *J. Mater. Sci.* **44**, 5080–5094 (2009).
23. Zhang, S., Xia, R. & Shrout, T. R. Lead-free piezoelectric ceramics vs. *PZT? J. Electroceram.* **19**, 251–257 (2007).
24. Helke, G. & Lubitz, K. *Piezoelectricity* 89-130 (Springer, 2008).
25. Gubinyi, Z., Batur, C., Sayir, A. & Dynys, F. Electrical properties of PZT piezoelectric ceramic at high temperatures. *J. Electroceram.* **20**, 95–105 (2008).
26. Huang, Y. L. et al. Pulsed laser deposition of complex oxide heteroepitaxy. *Chin. J. Phys.* **60**, 481–501 (2019).
27. Martin, R. M. Piezoelectricity. *Phys. Rev. B.* **5**, 1607 (1972).
28. Sundar, V. & Newnham, R. E. Electrostriction and polarization. *Ferroelectrics* **135**, 431–446 (1992).
29. Jiang, J. et al. Flexible ferroelectric element based on van der Waals heteroepitaxy. *Sci. Adv.* **3**, e1700121 (2017).
30. Liu, H. J. et al. Flexible Heteroepitaxy of $CoFe_2O_4$/Muscovite Bimorph with Large Magnetostriction. *ACS Appl. Mater.* **9**, 7297–7304 (2017).
31. Landau, L. & Lifshitz, E. Electrodynamics of Continuous Media (Pergamon Press, 1960).
32. Rivera, J. P. A short review of the magnetoelectric effect and related experimental techniques on (multi-) ferroics. *Eur. Phys. J. B.* **71**, 299 (2009).
33. Chrisey, D. B. & Hubler, G. K. eds. Pulsed laser deposition of thin films, (1994).
34. Lowndes, D. H., Geohegan, D. B., Puretzky, A. A., Norton, D. P. & Rouleau, C. M. Synthesis of novel thin-film materials by pulsed laser deposition. *Science* **273**, 898–903 (1996).

## ACKNOWLEDGEMENTS

The Ministry of Science and Technology supports this work, Taiwan (Grant nos. MOST 110-2124-M-007-004) and the Center for Emergent Functional Matter Science of National Yang Ming Chiao Tung University from The Featured Areas Research Center Program within the framework of the Higher Education Sprout Project by the Ministry of Education (MOE) in Taiwan.

## AUTHOR CONTRIBUTIONS

Y.J.W. processed the sample growth, PV, MH loop, and ME measurements and analyzed the data. J.W.C. supervised the XRD results. Y.H.L. analyzed the cross-sectional TEM images. P.W.S. and Y.C.C. assisted with the PFM work. Y.B. retouched the article. Y.J.W. and Y.H.C. conceived the idea, led the project, analyzed data, and co-wrote the paper. All the authors contributed to the manuscript.

## COMPETING INTERESTS

The authors declare no competing interests.

## ADDITIONAL INFORMATION

**Supplementary information** The online version contains supplementary material available at https://doi.org/10.1038/s41528-023-00241-8.

**Correspondence** and requests for materials should be addressed to Ying-Hao Chu.

**Reprints and permission information** is available at http://www.nature.com/reprints

**Publisher's note** Springer Nature remains neutral with regard to jurisdictional claims in published maps and institutional affiliations.